An experimental validation of the adoption of dc-dc converters for the impedance measurement in Li-Ion batteries

Andrea Zilio, Paolo Mattavelli
Department of Management and Engineering
University of Padova, Italy
andrea.zilio.5@studenti.unipd.it, paolo.mattavelli@unipd.it

***Abstract*—Electrochemical Impedance Spectroscopy (EIS) is one possible technique to determine the State of Health (SOH) in Li-Ion batteries. This article describes some challenges involved in the implementation of EIS analysis in a battery charger. As an application example, some design issues on the control of power converters that can be used to perform the EIS analysis are addressed. The description focuses on several aspects, from the development of the measurement channels for current and voltage to the design of the perturbation signal control system. The device performances are tested in several conditions such as to determine the impedance of a singular Li-ion cell having 3.63 V and 2.6 Ah , but also in a small-scale battery pack having 25.2 V and 11.2 Ah, using different perturbation signals.**

***Keywords*—Electrochemical Impedance Spectroscopy, Li-Ion Battery, Battery Impedance, Power Electronics Converter, Battery Charger.**

I. Introduction

The spreading of electric vehicles is a fundamental point to contrast the climate change and to allow a CO_2 emissions reduction [1]. However, there are many challenges to be solved to allow the spread of electric vehicles such as charging infrastructure as well as Li-Ion battery and powertrain efficiency.

Relevant progresses have been made over the last years to improve the Li-Ion batteries performance [2] and their energy density thanks to new manufacturing techniques [3].

Despite the impressive advancements in battery performance, some relevant improvements are still needed in the measurement and estimation of battery parameters. A more accurate state estimation of the battery internal conditions would allow, on the one hand, a better power management and, on the other hand, to implement new preventive maintenance techniques. The most important parameters to determine the battery conditions are the State of Charge (SOC) [4] and the State of Health (SOH). In the literature, several techniques have been implemented to determine the SOH. In [5], a technique based on energy level has been used, which, despite being fast, cannot be implemented on online operations [6]. Other advanced techniques are based on Kalman Filter [7] or on artificial intelligence [8]. They are very accurate but require a high computational effort [6].

Recently, the EIS has been used to determine the SOH. It is a very powerful non-invasive measurement technique suitable for the characterization of a great variety of materials [9]. The main drawback is that it requires impedance measuring equipment, which is often expensive. The adoption of such dedicated equipment can be avoided either by using the Battery Management System (BMS) [10] or the power converter used as battery chargers. The power converter has been recently suggested as a possible solution to achieve EIS in commercial applications at a lower cost, since it is a standard component in electric vehicles or rapid charging stations [11].

In several studies, the power converter is used to determine the battery impedance. In [12] a DC current pulse is injected into the battery and the voltage response is collected. The obtained impedance is also sensitive to the amplitude, the pulse width, and its frequency resolution [13]. The unidirectional power converter used in [14] does not allow to inject zero average current and consequently is not used to perform the offline EIS analysis.

This article focuses on some challenges to carry out the EIS using the battery charger. As an application example, a bidirectional power converter that aims to perform impedance spectroscopy is used. Instead of using the current ripple generated by DC/DC converter as in [15], the EIS is carried out by injecting a sinusoidal current obtained by adding a perturbation to the PWM duty cycle signal. Some design issues related to sensing circuits and the analog-to-digital converter (ADC) resolutions are also discussed.

The EIS is briefly explained in Section II. In Section III the power converter used as the perturbation unit is explained, while in Section IV the current loop design is illustrated. Section V shows the experimental results in which the EIS device is tested under several conditions.

II. Principles of EIS measurements

The fundamental approach of all impedance measurement methods is to apply a limited sinusoidal excitation current to the system under investigation and collect its voltage response.

This work was jointly supported by the European Union's Horizon 2020 research and innovation programme, under the Electronic Components and Systems for European Leadership (ECSEL) Joint Undertaking, and from Germany, Slovakia, Netherlands, Spain, and Italy under grant agreement No. 876868.

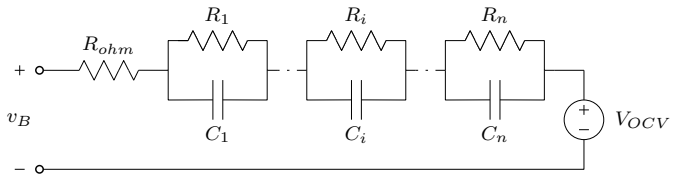

Fig. 1. Equivalent Battery Model with n RC cells.

The amplitude of the signal has to be such as to generate a linear response. The impedance of the system can be calculated as:

$$Z_B(j\omega) = \frac{v_B(j\omega)}{i_B(j\omega)} \tag{1}$$

where v_B is the battery voltage and i_B is the battery current perturbation.

The real and imaginary parts of the impedance are usually plotted in the Nyquist Plot. It gives a quick overview of the data and it is possible to make some qualitative and quantitative considerations. The equivalent electrical model of the battery can be represented in different configurations, order of the model, and accuracy. The most adopted one is a series connection of the ohmic resistive and of a series of parallel RC cells in which each cell represents a specific behavior [16]. For the scope of this paper, the initial model shown in Fig. 1 is simplified as the first-order RC circuit. The impedance of the first-order RC circuit can be computed as:

$$Z_{Batt}(s) = R_{ohm} + \frac{R_{ct}}{1 + sR_{ct}C_{ct}} \tag{2}$$

where R_{ohm} is the ohmic resistance, R_{ct} and C_{ct} are the charge transfer resistance and the capacity, respectively.

In [17] a method to determine and optimize the necessary parameters to perform useful EIS tests has been presented. The range of the frequency sweep depends on which phenomena are of interest, for example, at low frequency, the diffusive phenomena, while at high frequency the inductive ones [18].

III. Power Converter Uses as Perturbation Unit

Fig. 2 shows a possible power converter that can be used to charge the battery and which implements the impedance measurement. As an application example, a buck converter is adopted and it is provided with a power source to inject the current perturbation into the battery and two measurement channels to collect the current and voltage responses.

An external current loop has to be designed to control the current perturbation injected into the battery. Two currents can be used as feedback current. The first one is the inductor current i_L, but to perform the EIS analysis also the excitation current i_B has to be measured. The alternative is to carry out only the measurement of the battery current, which can be used for both control and EIS analysis.

A. Measurement channels

To perform the EIS analysis, there has to be two measurement channels. The first one is used to collect the voltage response v_B and the second one to measure the excitation current i_B. In Fig. 2 is also shown the voltage and current measurement channels.

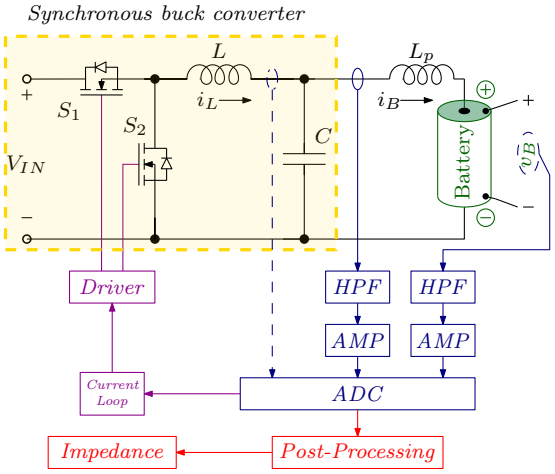

Fig. 2. Schematic circuit of the synchronous buck converter used for EIS analysis.

The main challenge is correlated with the limited impedance of a singular Li-Ion cell, thus all contact resistances must be minimized. To perform this task, a four-wire measurement method is implemented in the voltage channel. The voltage measurement has to be as close as possible to the battery terminals. It allows to eliminate from the measurement the effect of parasitic inductance introduced by the cables (L_p in Fig. 2).

To take full advantage of the conversion capabilities of the ADC, the voltage response has to be amplified. The amplification gain is chosen according to the impedance of the battery and the full scale value of the ADC.

Since the voltage perturbation is usually small, it is convenient to use the full-range scale of the ADC only for the AC component. Thus, the DC battery voltage shall be eliminated by means of a high pass filter (HPF). The HPF cut-off frequency is a trade-off between the response time and the attenuation at low frequencies. The same structure is implemented in the current channel.

IV. Current Control Design

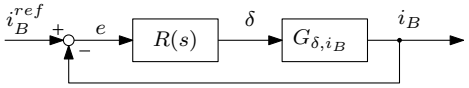

Fig. 3. Current Loop in continuous time domain.

To carry out the EIS analysis, the current perturbation has to be managed. To perform this task, a closed-loop current control is designed. The current perturbation is generated changing the duty cycle (δ) of the PWM signal, thus the transfer function between the battery current and the duty cycle has to be determined. The current loop in the continuous time domain is shown in Fig. 3.

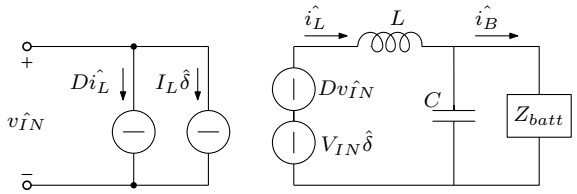

Fig. 4. Synchronous buck converter in which the small signal analysis is applied.

In the design of the controller, the battery parameters are unknown. They depends on many variables such as temperature, chemistry, battery form factor, and SOC. For this reason, a Proportional-Integral (PI) controller is used, the integral part allows to obtain a zero error in steady-state. In the literature, various studies have been performed and have resulted that there is a certain area in which the battery parameters can be found [19]. However, as discussed below, they are not strictly necessary for the current control design.

A. Transfer function between i_B and δ

Applying Time Averaging (TA) technique to the power converter dynamics and linearising the derived average model around the operating point, the Small-Signal (SS) model of the circuit of Fig. 2 is derived as shown in Fig. 4.

Applying the superposition principle, the transfer function between the inductor current (i_L) and the δ is:

$$G_{\delta,i_L}(s) = V_{IN}\frac{1 + sCZ_{Batt}}{Z_{Batt} + sL + s^2LCZ_{Batt}} \tag{3}$$

where L and C are the inductance and capacitance of the low pass filter, respectively.

From (3), the transfer function between the battery current (i_B) and the δ is:

$$G_{\delta,i_B}(s) = V_{IN}\frac{1}{Z_{Batt} + sL + s^2LCZ_{Batt}} \simeq \frac{V_{IN}}{sL} \tag{4}$$

Due to the fact that the battery impedance is limited, the transfer function can be written considering only the inductive effect.

B. PI design

For the synthesis of the controller, the Bode method is used. Defined $R(s)$ as the controller transfer function and $L(s) = R(s)G_{\delta,i_B}(s)$ as the open loop gain, a passband ω_g and a phase margin ϕ_m are used as design data. The following conditions must be satisfied::

$$\begin{cases} |L(j\omega_g)| = 1 \\ \pi + \angle L(j\omega_g) = \phi_m \end{cases} \tag{5}$$

The conditions imply that the PI regulator must compensate the lack of gain $\Delta K = 1/|L(j\omega_g)|$ and phase $\Delta\Phi = \phi_m - \pi - \angle L(j\omega_g)$ at the desired cross-over frequency. Thus, it is convenient to calculate the magnitude and phase of the system plant at the desired crossover frequency.

It is possible to calculate the PI parameters as:

$$\begin{cases} K_P = \Delta K\cos(\Delta\phi) \\ K_I = -\omega_g\Delta K\sin(\Delta\phi) \end{cases} \tag{6}$$

in which K_P and K_I are, respectively, the proportional gain and the integral gain of the controller.

In the application example, the controller is digitally implemented so it has to be discretized. The PI parameters for discrete implementation are obtained from the continuous design by substituting the variable *"s"* and applying the Euler backward method.

V. Experimental Results

The experimental setup is composed by two boards, the first one is the *Evaluation Board 6494L* designed by *STMicroelectronics* provided with two mosfets and their driver. The switching frequency is $210\,\mathrm{kHz}$ and is imposed through a PWM controller located in a custom board. The digital current control is developed in LabVIEW's environment. The sampling frequency is $50\,\mathrm{kHz}$ and, due to this high bandwidth, the entire control is developed in the National Instrument cRio's FPGA. The cRio is provided with 2 modules, the first one is the Analog-Digital Converter and the other one is the Digital-Analog Converter. The modules have the same specifications, $100\,\mathrm{kHz}$ as sampling frequency, $16\,\mathrm{bit}$ for the conversion and $\pm 10\,\mathrm{V}$ as full-scale value. A LabVIEW interface is used to generate and acquire the signals and to perform the FFT.

In the experimental setup there are two current measurement channels, one for the converter current control i_L and one for the battery current i_B. In the first one, a high accuracy is not required. In the second one, the sensing accuracy is relevant for the impedance measurement and a LEM current transducer with its appropriate calibration has been adopted.

The EIS analysis is carried out between $1\,\mathrm{Hz}$ and $1200\,\mathrm{Hz}$. The proposed approach can be used also for the battery impedance measurements at lower frequencies ($\simeq$mHz), if longer measurement time is possible. In our experiment, the test is performed by injecting one frequency at a time and measuring the response over multiple periods to ensure noise rejection.

Fig. 5 shows the device used to perform the EIS analysis. All tests are carried out using a Samsung's Li-ion battery cell ICR18650-26JM, and its specifications are shown in the Tab. I.

The tests are performed in the laboratory environment at ambient temperature.

A. Current loop test

The current control performance is tested. The reference signal is the summation of ten sinusoidal signals with $1\,\mathrm{A}$ as DC offset. The frequencies are $5, 10, 20, 50, 80, 120, 160, 350, 600, 800$ Hz, each sinusoidal has an amplitude of $0.05\,\mathrm{A}$. As reported in Fig. 6, there is an accurate tracking of the reference signal.

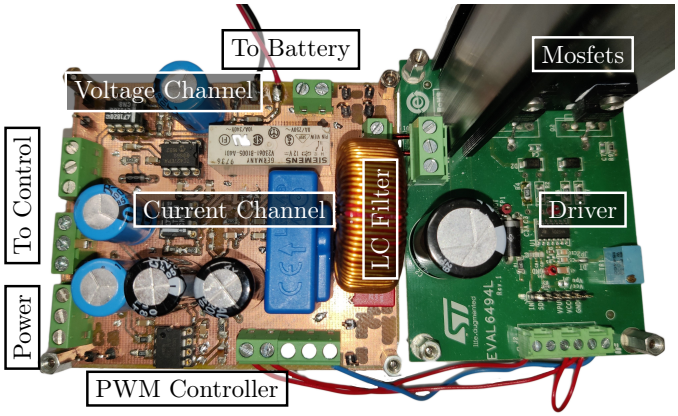

Fig. 5. Experimental setup used to perform the EIS analysis.

TABLE I
SPECIFICATIONS OF SAMSUNG'S LI-ION BATTERY CELL ICR18650-26JM.

Parameter	Value
Nominal voltage	3.63 V
Nominal Capacity	2600 mAh
Standard charge	CCCV, 1.3 A, 4.2 V, 8 mA cut-off
Rapid charge	CCCV, 2.6 A, 4.2 V, 8 mA cut-off
Max. continuous discharge	5.2 A
Discharge cut-off voltage	2.75 V

B. Measurement channel calibration

The transfer function between the input and the output of each measurement channel has to be determined to obtain the highest possible accuracy. This operation allows to calculate the gain and the phase at each frequency at which the test is carried out. These coefficients obtained are used to compensate the measure during the postprocessing operation. So the (2) can be write as:

$$Z_{REAL}(j\omega_i) = \frac{|v_B(j\omega)| \cdot G_v(j\omega)}{|i_B(j\omega)| \cdot G_i(j\omega)}$$

$$Z_{IMAG}(j\omega_i) = [\angle v_B(j\omega) - P_v(j\omega)] - [\angle i_B(j\omega) - P_i(j\omega)] \quad (7)$$

where $G_v(j\omega)$ and $P_v(j\omega)$ are the module and phase compensation coefficients for the voltage channel respectively, while $G_i(j\omega)$ and $P_i(j\omega)$ for the current channel.

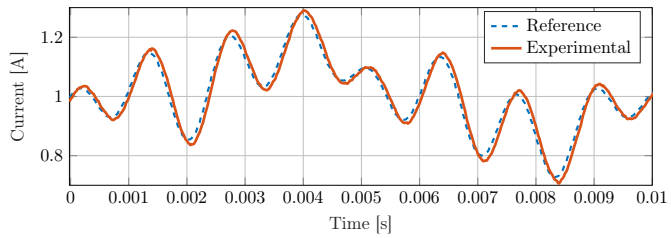

Fig. 6. Test of the current loop with a reference signal composed of the sum of 10 sinusoids $5, 10, 20, 50, 80, 120, 160, 350, 600, 800$ Hz with an amplitude of 0.05 A each and 1 A as DC offset.

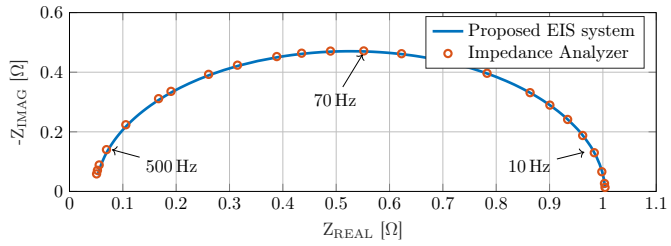

Fig. 7. Test of the EIS device in order to validate all aspects concerning its design.

C. Validation of EIS device

The EIS system is used to determine the impedance of a RC circuit at different frequencies for the purpose to validate the system itself, the LabVIEW interface, the measurement channels, and their calibration.

The RC circuit is composed by two power resistors (2 Ω each) in parallel configuration and a 2200 µF electrolytic capacitor. The excitation signal is composed of 155 frequencies between 1 Hz and 1200 Hz each of 0.2 A as amplitude with 0.3 A as DC offset. The *PSM1735 impedance analyzer* is used to determine the impedance of the circuit.

In [14] RMSE is used to validate the EIS system. It is calculated as:

$$RMSE = \sqrt{\sum_{i=1}^{M} \frac{\left(\left|Z_{fi}^{true}\right| - \left|Z_{fi}^{estimate}\right|\right)^2}{M}} \quad (8)$$

where M is the number of measures, Z_{fi}^{true} is the true impedance obtained through the impedance analyzer while $Z_{fi}^{estimate}$ is the impedance obtained from EIS device.

The impedance analyzer is set in such a way that its excitation signal has the same characteristics of the perturbation current to achieve the same effect. Under this hypothesis, the RMSE is 1.4 mΩ.

D. Low resolution ADC

To verify the EIS system and its accuracy on a low cost device, a test is performed using only 10 bits of the ADC.

By changing the number of bits of the acquisition variables, the same LabVIEW interface is used to compare the results that can be obtained with a 16-bit and 10-bit ADC.

The full capabilities of the 16-bit ADC allow to obtain a resolution of 0.305 mV (±10 V as full scale), while the resolution with 10-bit ADC is 15.6 mV (±8 V as full scale). The results shown that the RMSE between the two resolutions is 640 µΩ, therefore the error is negligible. The low RMSE is obtained thanks to the high gains of the instrumentation amplifiers that allow to exploit all ADC bits.

E. Performance validation

Several tests are carried out to verify the device. It is used to determine the battery impedance under several conditions.

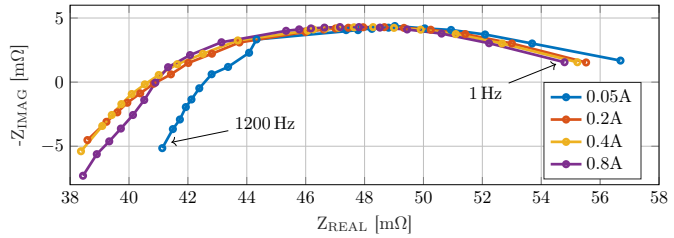

Fig. 8. EIS test performed in a singular Li-Ion cell with different current amplitude and without DC offset. The test is carried out in 21 points between 1 Hz and 1.2 kHz

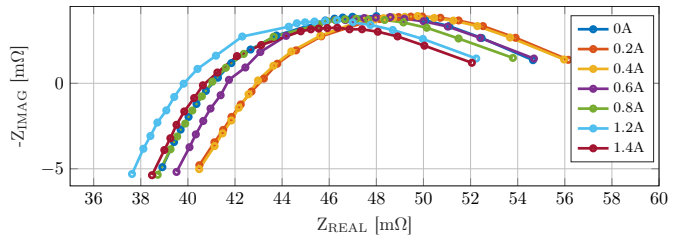

Fig. 9. EIS test performed in a singular Li-Ion cell at the same current amplitude using several DC offsets. The test is carried out in 21 points between 1 Hz and 1.2 kHz.

1) Amplitude effect: In Fig. 8 several measures are performed to determine the battery impedance using different current amplitudes. In the literature, there is no absolute indication of the minimum excitation current [17]. The limit is imposed by the measurement instrumentation and it depends on the minimum voltage response that can be acquired. With an amplitude of 0.05 A the minimum voltage response, amplified by 45 times, is 78 mV. Due to the fact that the switching noise is almost comparable to the voltage response, the measure is inaccurate and therefore the impedance trend is wrong.

The test is carried out also with the amplitude of 0.2 A, 0.4 A and 0.8 A the trend being slightly different due to the fact that the battery parameters depend on the amplitude of the excitation current [17]. Using a higher current perturbation (relative to cell capacity) can improve signal to noise ratio. However, some provisions are needed to ensure that the response remains in the linear regime, and that the internal temperature of the cell is not affected significantly by larger current amplitudes [20].

2) DC Offset effect: The effect of a DC offset superimposed on the current perturbation is taken into consideration. Its effect is shown in Fig. 9. The trends are different from each other because the current offset, in addition to charge the cell, causes a temperature variation.

3) Battey State Of Charge dependence: Fig. 10 shows the dependence between the SOC and the impedance. The results are consistent with the trends reported in [18] and [20].

4) Cells in series: The EIS test is carried out in a small-scale battery pack. It is provided with 28 Panasonic's cells in a 7s4p configuration. The nominal voltage is 25.2 V and the nominal capacity is 11.2 Ah. A BMS is used to balance the cells during the charging process and the excitation current

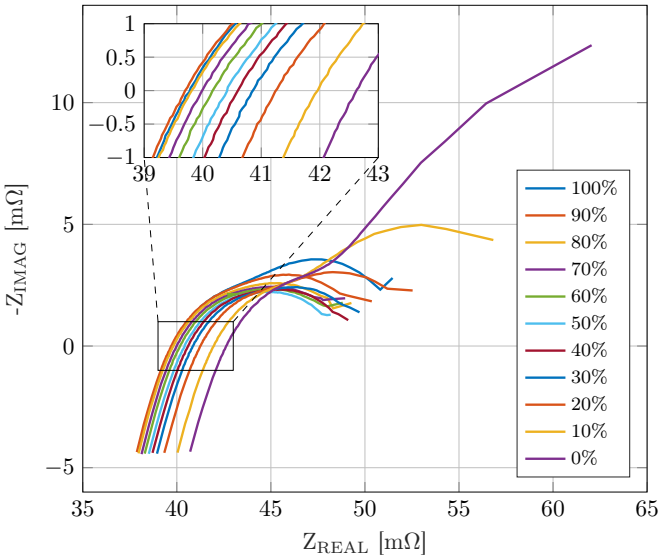

Fig. 10. EIS test performed in a singular Li-Ion cell at the same current amplitude (0.3 A) and without DC offset. The test is carried out in 155 points between 1 Hz and 1.2 kHz.

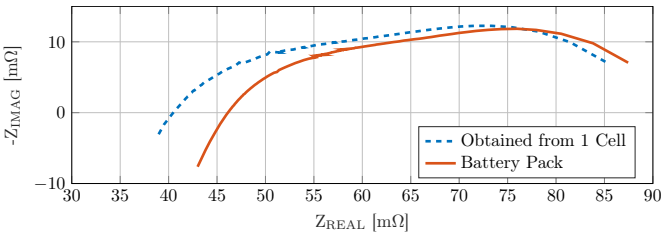

Fig. 11. Impedance of a small-scale battery in 7s4p configuration. The first one si obtained from a singular cell, and the second one from the EIS analysis performed using the battery pack The test is carried out in 155 points between 1 Hz and 1200 Hz. The perturbation signal has an amplitude of 0.5 A without DC offset.

flows through it. The result is reported in Fig. 11. The battery pack impedance can be determined also using the impedance of a singular cell but, as shown in Fig. 11, the results are different. This phenomenon is probably due to the contact resistances between the various cells.

5) Ageing test: An ageing test in two cylindrical cells is carried out to determine the battery impedance at different SOH conditions. The batteries are charged at 1 C-rate using the CC-CV algorithm and discharged at 1.5 C-rate. Every 50 cycles a slow discharge (0.5 C-rate) is performed to determine the capacity and therefore the SOH and EIS analysis is carried out. Fig. 12 shows the trend of the ohmic resistance as a function of the SOC and SOH. It is obtained by the intersection between Nyquist plot and the real axes.

VI. Conclusion

In this paper, some challenges to carry out the EIS analysis through the battery charger are been examined using an application example. Using an external current loop, the power convert has to be able to inject a current perturbation into the battery. The voltage measuring system is a fundamental

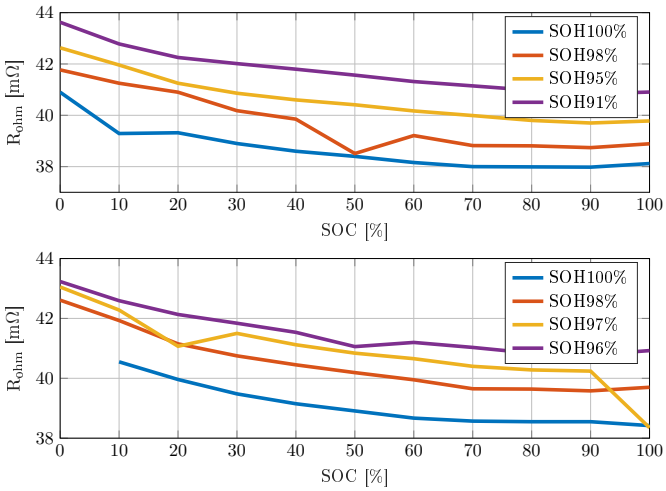

Fig. 12. Trend of ohmic resistance as a function of SOH in two different cells. It is obtained by carrying out an ageing test in two different Li-ion cylindrical cells.

point to achieve a high accuracy. It has to be placed as close as possible to the battery and has to implement a 4-wire measurement to remove the effect of parasitic elements.

In the application example, a bidirectional power converter in buck configuration mode is used. It can be used to perform the EIS analysis online and offline with good accuracy. The EIS system is used to determine the battery impedance under several conditions and a good accuracy is obtained even using ADC with 10 bits. The effect of the current amplitude of the perturbation signal and its correlation with the measurement noise were evaluated, and the DC offset and SOC effect are taken into consideration. The experimental results are consistent with those reported in the literature. The EIS system is used to determine the impedance of a 25.2 V-11.2 Ah battery pack.

References

[1] E. A. Nanaki and C. J. Koroneos, "Climate change mitigation and deployment of electric vehicles in urban areas," *Renewable energy*, vol. 99, pp. 1153–1160, 2016.

[2] M. Li, J. Lu, Z. Chen, and K. Amine, "30 years of lithium-ion batteries," *Advanced Materials*, vol. 30, no. 33, p. 1800561, 2018.

[3] J.-S. Kim, D.-C. Lee, J.-J. Lee, and C.-W. Kim, "Optimization for maximum specific energy density of a lithium-ion battery using progressive quadratic response surface method and design of experiments," *Scientific Reports*, vol. 10, no. 1, pp. 1–11, 2020.

[4] W. Kai, F. Xiao, P. Jinbo, R. Jun, D. Chongxiong, and L. Liwei, "State of charge (soc) estimation of lithium-ion battery based on adaptive square root unscented kalman filter," *Int. J. Electrochem. Sci*, vol. 15, pp. 9499–9516, 2020.

[5] J. Meng, L. Cai, D.-I. Stroe, G. Luo, X. Sui, and R. Teodorescu, "Lithium-ion battery state-of-health estimation in electric vehicle using optimized partial charging voltage profiles," *Energy*, vol. 185, pp. 1054–1062, 2019.

[6] N. Noura, L. Boulon, and S. Jemeï, "A review of battery state of health estimation methods: Hybrid electric vehicle challenges," *World Electric Vehicle Journal*, vol. 11, no. 4, p. 66, 2020.

[7] P. A. Topan, M. N. Ramadan, G. Fathoni, A. I. Cahyadi, and O. Wahyunggoro, "State of charge (soc) and state of health (soh) estimation on lithium polymer battery via kalman filter," in *2016 2nd International Conference on Science and Technology-Computer (ICST)*, 2016, pp. 93–96.

[8] J. Kim, H. Chun, M. Kim, J. Yu, K. Kim, T. Kim, and S. Han, "Data-driven state of health estimation of li-ion batteries with rpt-reduced experimental data," *Ieee Access*, vol. 7, pp. 106 987–106 997, 2019.

[9] D. D. Macdonald, "Reflections on the history of electrochemical impedance spectroscopy," *Electrochimica Acta*, vol. 51, no. 8-9, pp. 1376–1388, 2006.

[10] E. Din, C. Schaef, K. Moffat, and J. T. Stauth, "Online spectroscopic diagnostics implemented in an efficient battery management system," in *2015 IEEE 16th Workshop on Control and Modeling for Power Electronics (COMPEL)*. IEEE, 2015, pp. 1–7.

[11] R. Ferrero, C. Wu, A. Carboni, S. Toscani, M. De Angelis, H. George-Williams, E. Patelli, and P. A. Pegoraro, "Low-cost battery monitoring by converter-based electrochemical impedance spectroscopy," in *2017 IEEE International Workshop on Applied Measurements for Power Systems (AMPS)*. IEEE, 2017, pp. 1–6.

[12] P. Kollmeyer, A. Hackl, and A. Emadi, "Li-ion battery model performance for automotive drive cycles with current pulse and eis parameterization," in *2017 IEEE Transportation Electrification Conference and Expo (ITEC)*, 2017, pp. 486–492.

[13] I. Peláez, P. García, G. Villa, and S. Saheed, "Li-ion batteries parameter estimation using converter excitation and fusion methods," in *2019 IEEE Energy Conversion Congress and Exposition (ECCE)*. IEEE, 2019, pp. 2491–2498.

[14] E. Sadeghi, M. H. Zand, M. Hamzeh, M. Saif, and S. M. M. Alavi, "Controllable electrochemical impedance spectroscopy: From circuit design to control and data analysis," *IEEE Transactions on Power Electronics*, vol. 35, no. 9, pp. 9933–9942, 2020.

[15] Z. Xia and J. A. A. Qahouq, "High frequency online battery impedance measurement method using voltage and current ripples generated by dc-dc converter," in *2020 IEEE Applied Power Electronics Conference and Exposition (APEC)*. IEEE, 2020, pp. 1333–1338.

[16] U. Westerhoff, K. Kurbach, F. Lienesch, and M. Kurrat, "Analysis of lithium-ion battery models based on electrochemical impedance spectroscopy," *Energy Technology*, vol. 4, no. 12, pp. 1620–1630, 2016.

[17] Y. F. Pulido, C. Blanco, D. Anseán, V. M. García, F. Ferrero, and M. Valledor, "Determination of suitable parameters for battery analysis by electrochemical impedance spectroscopy," *Measurement*, vol. 106, pp. 1–11, 2017.

[18] D. I. Stroe, M. Swierczynski, A. I. Stan, V. Knap, R. Teodorescu, and S. J. Andreasen, "Diagnosis of lithium-ion batteries state-of-health based on electrochemical impedance spectroscopy technique," in *2014 IEEE Energy Conversion Congress and Exposition (ECCE)*. IEEE, 2014, pp. 4576–4582.

[19] S. M. M. Alavi, A. Mahdi, S. J. Payne, and D. A. Howey, "Identifiability of generalized randles circuit models," *IEEE Transactions on Control Systems Technology*, vol. 25, no. 6, pp. 2112–2120, 2017.

[20] N. Meddings, M. Heinrich, F. Overney, J.-S. Lee, V. Ruiz, E. Napolitano, S. Seitz, G. Hinds, R. Raccichini, M. Gaberšček *et al.*, "Application of electrochemical impedance spectroscopy to commercial li-ion cells: A review," *Journal of Power Sources*, vol. 480, p. 228742, 2020.